

LETTER TO THE EDITOR

PS J2107–1611: A new wide-separation, quadruply imaged lensed quasar with flux ratio anomalies

Frédéric Dux^{1,3}, Cameron Lemon¹, Frédéric Courbin¹, Dominique Sluse², Alain Smette³,
Timo Anguita^{4,5}, and Favio Neira^{1,4}

¹ Institute of Physics, Laboratoire d'Astrophysique, École Polytechnique Fédérale de Lausanne (EPFL), Observatoire de Sauverny, 1290 Versoix, Switzerland
e-mail: frederic.dux@epfl.ch

² STAR Institute, University of Liège, Quartier Agora – Allée du six Août, 19c, 4000 Liège, Belgium

³ European Southern Observatory, Alonso de Córdova 3107, Vitacura, Santiago, Chile

⁴ Instituto de Astrofísica, Facultad de Ciencias Exactas, Universidad Andres Bello, Av. Fernandez Concha 700, Las Condes, Santiago, Chile

⁵ Millennium Institute of Astrophysics, Monseñor Nuncio Sotero Sanz 100, Oficina 104, 7500011 Providencia, Santiago, Chile

Received 10 October 2023 / Accepted 13 October 2023

ABSTRACT

We report the discovery of PS J2107–1611, a fold-configuration 4.3''-separation quadruply lensed quasar with a bright lensed arc. It was discovered using a convolutional neural network on Pan-STARRS *gri* images of pre-selected quasar candidates with multiple nearby Pan-STARRS detections. Spectroscopic follow-up with EFOSC2 on the ESO 3.58 m New Technology Telescope reveals the source to be a quasar at $z = 2.673$, with the blended fold image pair showing deformed broad lines relative to the other images. The flux ratios measured from optical to near-infrared imaging in the Canada-France-Hawaii Telescope Legacy Survey, Pan-STARRS, the Legacy Surveys, and the Vista Hemisphere Survey are inconsistent with a smooth mass model as the fold pair images are ~ 15 times too faint. Variability, time delay effects, and reddening are ruled out through multiple-epoch imaging and color information. The system is marginally resolved in the radio in the Very Large Array Sky Survey *S*-band, where it has a 10 mJy detection. The radio flux ratios are compatible with the smooth mass macromodel. This system offers a unique tool for future studies of quasar structure with strong and microlensing. A more detailed analysis of follow-up with JWST/MIRI, VLT/MUSE, VLT/ERIS, and data from the European Very Long Baseline Interferometer will be presented in a forthcoming paper.

Key words. gravitational lensing: strong – galaxies: active

1. Introduction

Strongly lensed quasars, that is multiply imaged luminous active galactic nuclei (AGN) at cosmological distances, have been used extensively to address a broad range of astrophysical and cosmological phenomena. They are powerful probes of cosmological parameters, either in large statistical samples (e.g., Chae 2003) or individually through for example time-delay cosmography (e.g., Refsdal 1964; York et al. 2005; Wong et al. 2020). They aid in constraining the lens galaxy mass distribution, from the largest spatial scales (e.g., Oguri et al. 2014) down to the scale of dark matter substructure (e.g., Nierenberg et al. 2017). They have been used to constrain the initial mass function of lens galaxies (e.g., Schechter et al. 2014) through microlensing, the additional lensing effect on the quasar images by stars in the lensing galaxy. Microlensing in lensed quasars enables a powerful probe of the inner quasar source structure: the X-ray emitting region (e.g., Chartas et al. 2009), the accretion disk size and its temperature profile (e.g., Jiménez-Vicente et al. 2014), and the geometry of the broad-line region (BLR, e.g., Hutsemékers et al. 2019; Hutsemékers & Sluse 2021; Paic et al. 2022). Finally, optical studies of the central kiloparsecs of quasar host galaxies at high-redshift are only possible with strongly

lensed quasars as the host is not only amplified but also well-separated from the bright quasar images, observed as bright arcs (e.g., Bayliss et al. 2017).

These science cases are currently hindered by the still limited number of confirmed lensed quasars, in particular quadruply imaged systems (quads), of which only ~ 60 are currently known (Lemon et al. 2023). A special sub-sample of quads are those that display radio emission; they can probe radio emission at high-redshift (e.g., Badole et al. 2022), yield microlensing- and dust-free flux ratios, and very-long-baseline Interferometry (VLBI) follow-up of such systems provide unprecedented datasets for constraining the lens galaxy mass (Spingola et al. 2018; Powell et al. 2022). Only $\mathcal{O}(10)$ radio-loud quads are known, most of them discovered over 20 years ago by the Cosmic Lens All Sky Survey (CLASS) and the Jodrell Bank VLA Astrometric Survey (JVAS, Myers et al. 2003; Browne et al. 2003). Since then, all quads discovered have been in the optical with only faint radio counterparts (Hartley et al. 2021, Table 5).

Here, we report the discovery of an unusual new quad, discovered using a convolutional neural network (CNN) specifically designed to find well-separated quads in Pan-STARRS (PS) imaging data. This is the first discovery of a lensed quasar with a CNN. In this letter, we attempt to explain the unusual configuration of

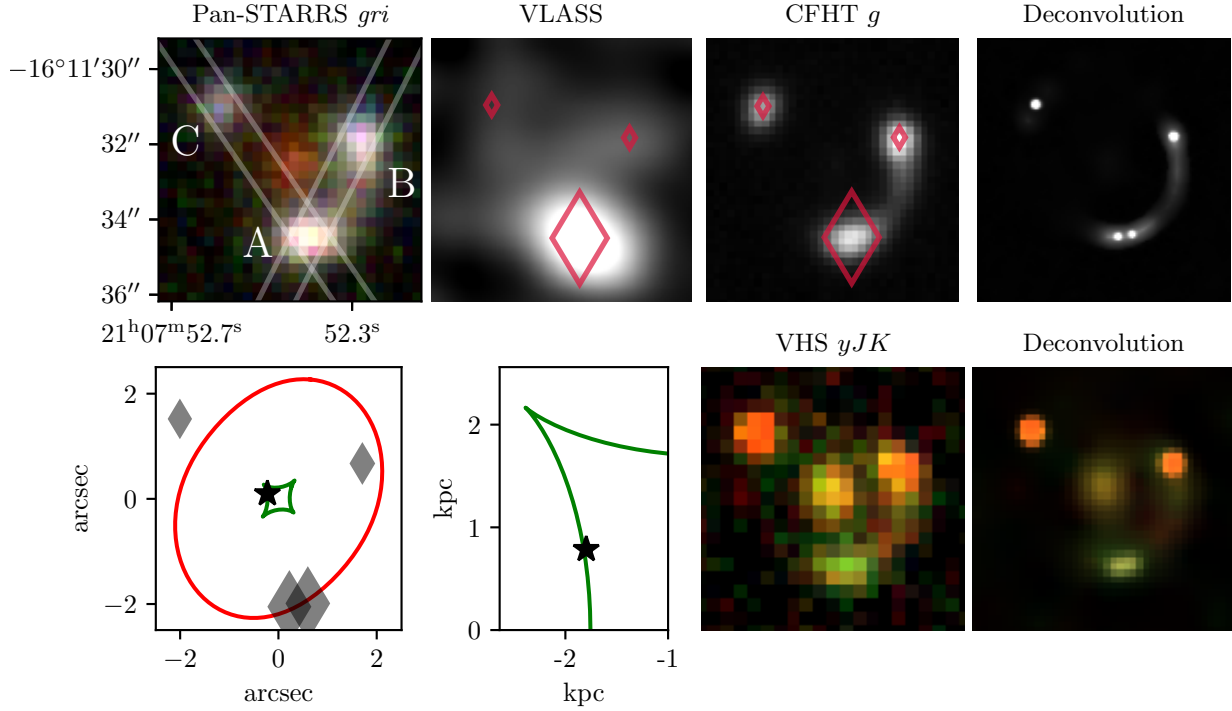


Fig. 1. Overview of the available imaging data and the inferred smooth mass macro model. *Top:* Pan-STARRS *gri* image, with the lensed images labeled and the two EFOSC2 slit positions used for the discovery spectra, followed by the VLASS radio map and the CFHT optical images. The last panel shows a deconvolution of the CFHT image with STARRED (see text). The two central images are overlaid with markers of area proportional to the predicted relative magnifications from our smooth mass macro model of the lens. *Bottom:* mass model constrained using only the astrometry of the lensed images as derived with the CFHT data. A zoom on the point source position and the caustic in the source plane is shown on the second panel. The VHS *yJK* image is shown on the third panel, followed by its STARRED deconvolution showing a noticeable dimming of the merging pair with wavelength in the near-IR when compared to the optical imaging.

this quad through an analysis of available archival imaging data and new imaging and spectroscopy. We explain our method of discovery in Sect. 2 and present the available data and follow-up spectroscopy in Sect. 3. We briefly draw conclusions from our analysis and state our future plans in Sect. 4.

Throughout this letter we assume a flat Λ CDM cosmology with $H_0 = 70 \text{ km s}^{-1} \text{ Mpc}^{-1}$ and $\Omega_m = 0.3$.

2. Discovery method

The Pan-STARRS 3π survey provides 1 arc-second seeing *grizY* imaging of the entire sky north of a declination of $\delta = -30^\circ$ (Chambers et al. 2016). This is an ideal dataset for finding bright gravitationally lensed quasars given its $r \sim 22$ depth (5σ), which aptly matches the brightness of quasar samples from many surveys, such as *Gaia* (e.g., Shu et al. 2019).

Our initial catalog is version 6.6¹ of MILLIQUAS (Flesch 2021), which contains confirmed and candidate quasars compiled from the literature and recent quasar catalogs. To look for possible lensed systems, we cross-matched to the Pan-STARRS catalog, requiring two or more detections within $5''$, resulting in 27 760 candidates, including 70 known lenses.

We trained a CNN on mock quad lensed quasars to identify promising candidates. CNNs have been shown to be an effective method on recovering quads in mock datasets (Akhazhanov et al. 2022). Our mocks were built using the image and galaxy positions and *i*-band brightnesses provided in the catalogs of Oguri & Marshall (2010). To evaluate the K-corrections

in the *g* and *r* bands, we used the catalog source and lens redshifts, and measured the corrections for the relevant filters using redshifted quasar and galaxy templates from Vanden Berk et al. (2001) and Kinney et al. (1996) respectively. We did not include any reddening or microlensing effects. The light of the lens galaxy was represented as a Sérsic profile (Sérsic 1963), and the quasar images as point sources. Each image was then convolved with a Moffat (Moffat 1969) profile representing the point spread function (PSF) with widths varying from 0.9 to 1.2 arcseconds. Finally, Poisson and Gaussian noise was added. For the negative examples, we used random systems with multiple detections in Pan-STARRS and with magnitudes matching those of our quasar sample.

The details of the training steps, CNN architecture, and application to updated quasar catalogs will be presented in an upcoming paper. We ran the CNN on $10''$ Pan-STARRS *gri* cutouts of the candidates centered on the MILLIQUAS catalog position. We then visually inspected the cutouts of the 2000 best-scoring candidates, selecting 131 promising ones. Among those, we recovered 13 known quads, 23 doubles, and the new likely quad system PS J2107–1611, whose Pan-STARRS *gri* image is displayed in the first panel of Fig. 1. The system displays three point-like components surrounding an extended object, with a clear arc visible between images A and B. We estimate its total magnitude to *g* = 19.4 and *i* = 18.4. This is one of the brightest lensed arcs of all galaxy-scale lensed quasars.

3. Follow-up and archival data

We acquired long-slit spectroscopy of PS J2107–1611 with EFOSC2 on the ESO 3.58 m New Technology Telescope (NTT)

¹ <https://heasarc.gsfc.nasa.gov/w3browse/all/milliquas.html>; from 14 June 2020.

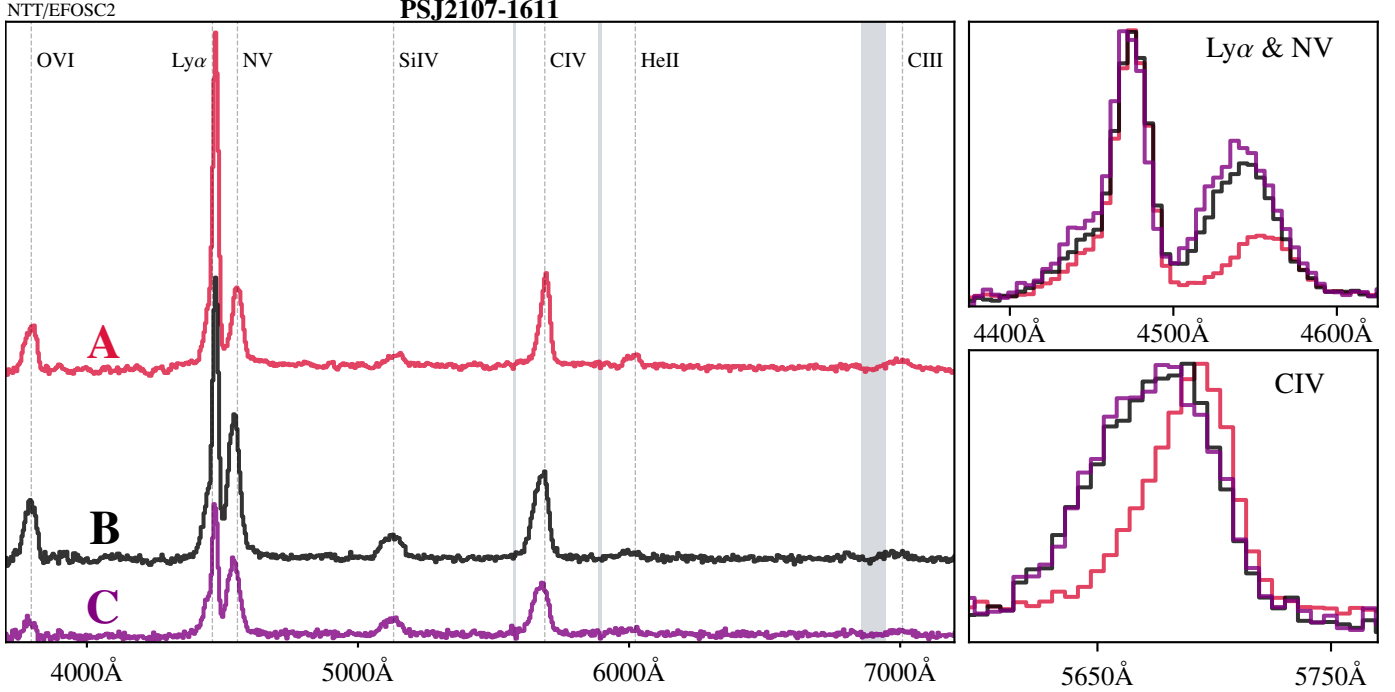


Fig. 2. EFOSC2 spectra of the three visible lensed images of PS J2107-1611. The A spectrum is the average of the individual spectra extracted from the two slit angles shown in Fig. 1. *Left:* complete spectra with fluxes shifted for display purposes. *Right:* zoom-ins on the Ly α , NV and CIV emission lines. The zoomed-in regions are normalized to their maximum intensity to highlight the larger skewness in these two lines of the A spectrum.

in October 2020². Two exposures were taken with a 1.0'' slit and grism #13 ($R \sim 260$), at position angles of PA = -34.3° and PA = 26.6° east of north, as shown in the first panel of Fig. 1. The Differential Image Motion Monitor (DIMM) seeing was roughly 1.2'' throughout the exposures.

The spectra were extracted as described in Lemon et al. (2023), providing modelled deblended spectra for two point sources along each slit. Since A was in both slit angles, we validated our extraction algorithm by checking that the independently extracted spectra of A matched within the noise, which they did. The three spectra are typical of a quasar at $z_s \sim 2.673$ (Fig. 2, where the two spectra of image A have been averaged). Images B and C are very similar with a flux ratio B/C of ~ 1.8 , approximately constant with wavelength and compatible with 2 images of the same object with differences attributable to extrinsic effects (e.g., microlensing). There are, however, clear differences in the shapes of the NV and CIV lines of A relative to B and C, as shown in the peak-normalized zoom-ins on the right panels of Fig. 2. We also note the presence of clear residuals in the 2D A-B spectrum, between the two quasar images, at a wavelength corresponding to Ly α (Fig. 3). We attribute this to the lensed host galaxy already seen in imaging data.

To better understand the nature of this system, we analyzed available archival imaging. In particular we found deep g -band Canada-France-Hawaii Telescope (CFHT) data with a total exposure time of 6901 seconds, an average seeing of 0.81'' and a pixel size of 0.187''. We measured the astrometry of the different components using the two-channel image deconvolution algorithm STARRED (Michalewicz et al. 2023). This algorithm models the bright point sources and a wavelet-regularized background as two channels and fits them jointly to the data. This idea has been shown to be very effective in doing precise

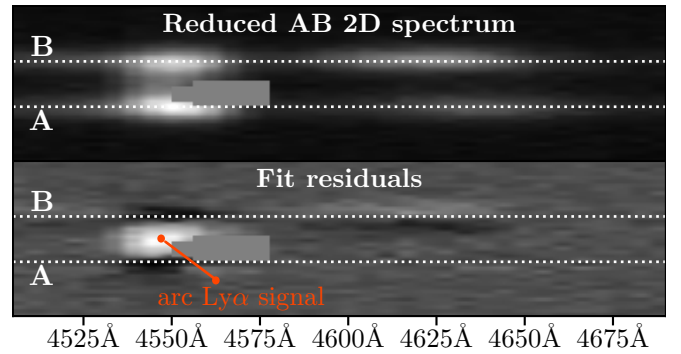


Fig. 3. EFOSC2 2D spectrum for the slit orientation on images A and B. The Ly α emission line associated to the lensed quasar host galaxy is clearly detected between the A and B images. The arc is made visible after subtraction of the two point sources, in the bottom panel.

photometry of blended point sources superposed on a complex background, namely, the lensed quasars images, the lens galaxy, and the lensed quasar host galaxy in strongly lensed systems. Based on the MCS deconvolution method (Magain et al. 1998), STARRED is the new method used to extract light curves of lensed quasars in the context of the COSMOGRAIL program (see, e.g., Million 2020).

Guided by preliminary lens models of the system and by the poorer quality of deconvolutions with three point-sources, we elected a model with four point-sources, which is also a general feature of all realistic lensing potentials (Burke 1981). Image A is well compatible with being a blend of two images, A₁ and A₂, arising due to a source in fold configuration. A single exposure of the CFHT dataset and the four point-source deconvolution is shown at the top-right of Fig. 1. We take this as our fiducial deconvolved model as there is good evidence for it from both

² P.I.: Timo Anguita, 106.218K.001.

Table 1. Astrometry of the CFHT deconvolution, given for each point source relative to the lensing galaxy centered on RA(2000): 21h07m52.4s and Dec(2000): $-16^{\circ}11'32.4''$ (ICRS).

	$\Delta\alpha \cos \delta [']$	$\Delta\delta [']$	Magnification	Δt [days]
A ₁	0.217	-2.056	-33	0
A ₂	0.593	-1.993	36	0.05
B	1.703	0.668	-4	20
C	-2.010	1.515	4	-79

Notes. We also include the magnification and time delays predicted by a mass model with a fiducial lens redshift of $z_l = 0.5$ and constrained using this astrometry (see text). The point sources are labeled counter-clockwise.

the lens model and the smooth resulting background arc. However, we note that higher resolution imaging is needed to confirm the fold pair.

Next, we used the astrometry of the fiducial model given in Table 1 to constrain a lensing mass model of a singular isothermal ellipsoid with external shear with LENSTRONOMY (Birrer & Amara 2018; Birrer et al. 2021). We did not use the flux ratios, and we fixed the lens galaxy position to the centroid of the light as measured from the available *i*-band imaging data. The fit optimization was done in the source plane with each image weighted equally. The resulting total magnification is 78 with an *Einstein* radius of $2.12''$. The ellipticity is 0.2 at 67 degrees east of north, and the external shear strength is 0.06 at 115 degrees east of north. The individual magnifications are also plotted in the top-central panels of Fig. 1, illustrating the relative flux discrepancy and compatibility in the optical and radio, respectively.

We provide flux ratio estimates between the three visible point-sources (summing A₁ and A₂ together as A) measured from Pan-STARRS *grizY*, Legacy Survey (LS) *i*, and VHS (VISTA Hemisphere Survey, McMahon et al. 2013) images. Due to the degeneracy between the flux originating from the ring and from the point sources, we measured the fluxes in the point sources with two methods: (i) with a STARRED deconvolution, where a part of the total flux is absorbed by the wavelet-representation of the arc, and (ii) with standard PSF photometry, where all the flux, including that of the arc, goes into the point sources. The two values provide a plausible range where the true flux values of the point sources should lie. The filter, date, and B-A and C-A magnitude differences are listed in Table 2. The optical flux ratios are fairly constant across wavelength, followed by a decrease of the relative flux of A in the near-infrared bands. In Fig. 1 we also show the Very Large Array Sky Survey image (VLASS, Lacy et al. 2020), which reveals that the brightest radio component is centred on A. We estimate a flux ratio of ~ 15 -to-1 between A and B, but this is highly uncertain given the large effective beam size and blending of the system.

4. Discussion and conclusions

Deformed broad lines as seen in the blended spectrum of image A relative to images B and C have been observed previously in other lensed quasars and attributed to microlensing (e.g., Richards et al. 2004; Sluse et al. 2011). Studying the lines shapes in future spectra will be a good test of this, as changing shapes would be consistent with the variable nature of microlensing. Microlensing is also a natural explanation of the highly discrepant measured flux ratios as compared with a

Table 2. Flux ratios measured on the optical images.

Band	Dataset	Epoch	Δmag	
			B – A	C – A
<i>g</i>	CFHT	2004-07-23	-0.3 (0.4)	-0.2 (1.0)
<i>r</i>	PS	2009-2014	0.4 (0.2)	0.5 (1.0)
<i>i</i>	PS	2009-2014	0.6 (0.4)	0.5 (1.2)
<i>i</i>	LS	2020-2021	0.5 (0.3)	0.6 (1.1)
<i>Y</i>	VHS	2014-04-15	0.4 (0.6)	0.3 (1.1)
<i>J</i>	VHS	2014-04-15	-0.1 (0.5)	-0.6 (0.6)
<i>Ks</i>	VHS	2014-04-15	-1.7 (-0.6)	-2.1 (-0.9)

Notes. Two values are reported: the first stems from a STARRED deconvolution (PSF + wavelet background ring). The second, in parenthesis, stems from standard PSF photometry that sums the flux of the quasar images and the flux of the underlying arc (see text).

smooth mass macromodel, although both the saddle point and minimum of the fold pair are 15 times too faint, which would be extremely unlikely (see, e.g., Weisenbach et al. 2021). However, we must keep in mind that the image fluxes and positions from our deconvolution are prone to systematic uncertainty, given the limited seeing of the original data, and the image pair could indeed have very different fluxes. The marginally-resolved radio image of the system, however, does show flux ratios that agree with our best lens model, and should not (in principle) suffer from microlensing given the much larger emission regions in the radio than in the optical/IR.

Several other effects are suggested to modify lensed images flux ratios: (i) dust reddening, however, this is not a plausible explanation given the similar optical colors; (ii) a combination of variability and time delay effect, also an unlikely explanation given the lack of variability seen in individual Pan-STARRS epochs spanning several years (coupled with an estimated time delay of about 80 days); (iii) dark matter substructure (e.g., McKean et al. 2007); and (iv) finite source size effects coupled with differential magnification such as the radio source being well separated from the optical and infrared source (see, e.g., Barnacka 2018; Zhang et al. 2023). It is likely that the latter two explanations possibly coupled with microlensing could explain the data, given that the source is constrained to be close to the caustic, potentially parsecs away, with a macro-magnification around 70.

Further observations are required to fully understand PS J2107–1611 at high spatial resolution and with broad wavelength coverage and spectroscopy. Future works will present the analysis of such additional datasets of this system, including JWST/MIRI, VLT/MUSE 2D spectra, VLT adaptive optics with the ERIS instrument, and in the radio with the European Very Long Baseline Interferometer (Lemon et al., in prep.).

Acknowledgements. This program is supported by the Swiss National Science Foundation (SNSF) and by the European Research Council (ERC) under the European Union’s Horizon 2020 research and innovation program (COSMICLENS: grant agreement No 787886). TA acknowledges support from the Millennium Science Initiative ICN12_009 and the ANID BASAL project FB210003. Pan-STARRS: The Pan-STARRS1 Surveys (PS1) and the PS1 public science archive have been made possible through contributions by the Institute for Astronomy, the University of Hawaii, the Pan-STARRS Project Office, the Max-Planck Society and its participating institutes, the Max Planck Institute for Astronomy, Heidelberg and the Max Planck Institute for Extraterrestrial Physics, Garching, The Johns Hopkins University, Durham University, the University of Edinburgh, the Queen’s University Belfast, the Harvard-Smithsonian Center for Astrophysics, the Las Cumbres Observatory Global Telescope Network Incorporated, the National Central University of Taiwan, the Space Telescope Science

Institute, the National Aeronautics and Space Administration under Grant No. NNX08AR22G issued through the Planetary Science Division of the NASA Science Mission Directorate, the National Science Foundation Grant No. AST-1238877, the University of Maryland, Eotvos Lorand University (ELTE), the Los Alamos National Laboratory, and the Gordon and Betty Moore Foundation. CFHT: We made the use of observations obtained with MegaPrime/MegaCam, a joint project of CFHT and CEA/DAPNIA, at the CFHT which is operated by the National Research Council (NRC) of Canada, the Institut National des Sciences de l'Univers of the Centre National de la Recherche Scientifique (CNRS) of France, and the University of Hawaii. The observations at the Canada-France-Hawaii Telescope were performed with care and respect from the summit of Maunakea which is a significant cultural and historic site. VLASS: The National Radio Astronomy Observatory is a facility of the National Science Foundation operated under cooperative agreement by Associated Universities, Inc. CIRADA is funded by a grant from the Canada Foundation for Innovation 2017 Innovation Fund (Project 35999), as well as by the Provinces of Ontario, British Columbia, Alberta, Manitoba and Quebec. Legacy Surveys: The Legacy Surveys consist of three individual and complementary projects: the Dark Energy Camera Legacy Survey (DECaLS; Proposal ID #2014B-0404; PIs: David Schlegel and Arjun Dey), the Beijing-Arizona Sky Survey (BASS; NOAO Prop. ID #2015A-0801; PIs: Zhou Xu and Xiaohui Fan), and the Mayall z -band Legacy Survey (MzLS; Prop. ID #2016A-0453; PI: Arjun Dey). DECaLS, BASS and MzLS together include data obtained, respectively, at the Blanco telescope, Cerro Tololo Inter-American Observatory, NSF's NOIRLab; the Bok telescope, Steward Observatory, University of Arizona; and the Mayall telescope, Kitt Peak National Observatory, NOIRLab. Pipeline processing and analyses of the data were supported by NOIRLab and the Lawrence Berkeley National Laboratory (LBNL). The Legacy Surveys project is honored to be permitted to conduct astronomical research on Iolkam Du'ag (Kitt Peak), a mountain with particular significance to the Tohono O'odham Nation.

References

- Akhazhanov, A., More, A., Amini, A., et al. 2022, *MNRAS*, **513**, 2407
- Badole, S., Venkattu, D., Jackson, N., et al. 2022, *A&A*, **658**, A7
- Barnacka, A. 2018, *Phys. Rep.*, **778**, 1
- Bayliss, M. B., Sharon, K., Acharyya, A., et al. 2017, *ApJ*, **845**, L14
- Birrer, S., & Amara, A. 2018, *Phys. Dark Universe*, **22**, 189
- Birrer, S., Shajib, A. J., Gilman, D., et al. 2021, *J. Open Source Software*, **6**, 3283
- Browne, I. W. A., Wilkinson, P. N., Jackson, N. J. F., et al. 2003, *MNRAS*, **341**, 13
- Burke, W. L. 1981, *ApJ*, **244**, L1
- Chae, K.-H. 2003, *MNRAS*, **346**, 746
- Chambers, K. C., Magnier, E. A., Metcalfe, N., et al. 2016, arXiv e-prints [arXiv:1612.05560]
- Chartas, G., Kochanek, C. S., Dai, X., Poindexter, S., & Garmire, G. 2009, *ApJ*, **693**, 174
- Flesch, E. W. 2021, The Million Quasars (Milliquas) v7.2 Catalogue, now with VLASS associations. The inclusion of SDSS-DR16Q quasars is detailed [arXiv:2105.12985]
- Hartley, P., Jackson, N., Badole, S., et al. 2021, *MNRAS*, **508**, 4625
- Hutsemékers, D., & Sluse, D. 2021, *A&A*, **654**, A155
- Hutsemékers, D., Braibant, L., Sluse, D., & Goosmann, R. 2019, *A&A*, **629**, A43
- Jiménez-Vicente, J., Mediavilla, E., Kochanek, C. S., et al. 2014, *ApJ*, **783**, 47
- Kinney, A. L., Calzetti, D., Bohlin, R. C., et al. 1996, *ApJ*, **467**, 38
- Lacy, M., Baum, S. A., Chandler, C. J., et al. 2020, *PASP*, **132**, 035001
- Lemon, C., Anguita, T., Auger-Williams, M. W., et al. 2023, *MNRAS*, **520**, 3305
- Magain, P., Courbin, F., & Sohy, S. 1998, *ApJ*, **494**, 472
- McKean, J. P., Koopmans, L. V. E., Flack, C. E., et al. 2007, *MNRAS*, **378**, 109
- McMahon, R. G., Banerji, M., Gonzalez, E., et al. 2013, *The Messenger*, **154**, 35
- Michalewicz, K., Millon, M., Dux, F., & Courbin, F. 2023, *J. Open Source Software*, **8**, 5340
- Millon, M., et al. 2020, *A&A*, **642**, A193
- Moffat, A. F. J. 1969, *A&A*, **3**, 455
- Myers, S. T., Jackson, N. J., Browne, I. W. A., et al. 2003, *MNRAS*, **341**, 1
- Nierenberg, A. M., Treu, T., Brammer, G., et al. 2017, *MNRAS*, **471**, 2224
- Oguri, M., & Marshall, P. J. 2010, *MNRAS*, **405**, 2579
- Oguri, M., Rusu, C. E., & Falco, E. E. 2014, *MNRAS*, **439**, 2494
- Paic, E., Vernardos, G., Sluse, D., et al. 2022, *A&A*, **659**, A21
- Powell, D. M., Vegetti, S., McKean, J. P., et al. 2022, *MNRAS*, **516**, 1808
- Refsdal, S. 1964, *MNRAS*, **128**, 307
- Richards, G. T., Keeton, C. R., Pindor, B., et al. 2004, *ApJ*, **610**, 679
- Schechter, P. L., Pooley, D., Blackburne, J. A., & Wambsganss, J. 2014, *ApJ*, **793**, 96
- Sérsic, J. L. 1963, *Boletín de la Asociación Argentina de Astronomía La Plata Argentina*, **6**, 41
- Shu, Y., Kposov, S. E., Evans, N. W., et al. 2019, *MNRAS*, **489**, 4741
- Sluse, D., Schmidt, R., Courbin, F., et al. 2011, *A&A*, **528**, A100
- Spingola, C., McKean, J. P., Auger, M. W., et al. 2018, *MNRAS*, **478**, 4816
- Vanden Berk, D. E., Richards, G. T., Bauer, A., et al. 2001, *AJ*, **122**, 549
- Weisenbach, L., Schechter, P. L., & Pontula, S. 2021, *ApJ*, **922**, 70
- Wong, K. C., Suyu, S. H., Chen, G. C. F., et al. 2020, *MNRAS*, **498**, 1420
- York, T., Jackson, N., Browne, I. W. A., Wucknitz, O., & Skelton, J. E. 2005, *MNRAS*, **357**, 124
- Zhang, L., Zhang, Z.-Y., Nightingale, J. W., et al. 2023, *MNRAS*, **524**, 3671